Fuel 129 (2014) 129–137

Contents lists available at ScienceDirect

Fuel

journal homepage: www.elsevier.com/locate/fuel

Investigation of adsorption-enhanced reaction process of mercury removal from simulated natural gas by mathematical modeling

Carla Luciane Manske Camargo [a], Neuman Solange de Resende [a], Amanda Gerhardt de Oliveira [a], Vera Maria Martins Salim [a], Frederico Wanderley Tavares [a,b,*]

[a] Programa de Engenharia Química/COPPE, Universidade Federal do Rio de Janeiro, Cidade Universitária, Rio de Janeiro 21941-972, RJ, Brazil
[b] Escola de Química, Universidade Federal do Rio de Janeiro, Cidade Universitária, Rio de Janeiro 21949-900, RJ, Brazil

HIGHLIGHTS

- The proposed model for Hg fixation involves adsorption, diffusion and chemical reaction.
- Experimental data are obtained for low concentration in the gaseous stream.
- Chemical fixation of mercury inside the solid matrix leads to an increase of mercury removal capacity.
- Chemical fixation minimizes the risks of mercury re-emission to environment.

GRAPHICAL ABSTRACT

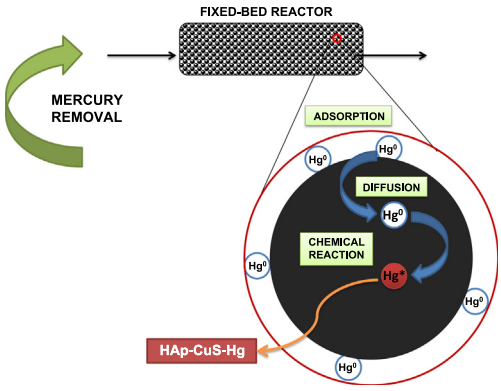

ARTICLE INFO

Article history:
Received 2 November 2013
Received in revised form 14 March 2014
Accepted 21 March 2014
Available online 4 April 2014

Keywords:
Mercury removal
Natural gas
Surface adsorption
Chemical fixation
Fixed bed simulation

ABSTRACT

Hydroxyapatites modified with copper sulfide were studied as sorbents for mercury removal from gaseous streams containing low mercury concentration. A mathematical model was proposed to take into account adsorption, diffusion into the sorbent particle and chemical reaction inside the solid matrix. The chemical reaction mechanism for mercury fixation into the solid matrix is supported by XRD analysis results. The unknown parameters are estimated from experimental data by minimization of the unweighted least-squares function, using a hybrid of Newton-like and Particle Swarm Optimization methods. Results are shown for two hydroxyapatite sorbents developed in our lab. The model, with its optimized parameters, was used to study the dynamic behavior of a fixed bed adsorption process at different operational conditions. Simulation results show that the chemical fixation of mercury inside the solid matrix leads to an increase of mercury removal capacity and it provides insights about operational plant conditions.

1. Introduction

Combustion of fossil fuels is the main way of mercury emission from anthropogenic sources, especially in coal-burning power plants [1–3]. Currently, mercury is considered as a "global pollutant" because it can be transported globally in its gaseous

* Corresponding author. Tel.: +55 21 2562 7650; fax: +55 21 2562 7567.
E-mail addresses: cmanske@peq.coppe.ufrj.br (C.L.M. Camargo), neuman@peq.coppe.ufrj.br (N.S. de Resende), agerhardt@peq.coppe.ufrj.br (A.G. de Oliveira), vera@peq.coppe.ufrj.br (V.M.M. Salim), tavares@eq.ufrj.br (F.W. Tavares).

http://dx.doi.org/10.1016/j.fuel.2014.03.048
0016-2361/

Nomenclature

C	mercury concentration in the fluid phase (kg m^{-3})
C_o	inlet mercury concentration (kg m^{-3})
$\bar{q}$	average amount of mercury inside the particles (kg m^{-3})
q_{RQ}	amount of mercury reacted at time t (kg m^{-3})
q_{RQm}	maximum amount of mercury fixed by solid (kg m^{-3})
q_{Rp}	amount of mercury adsorbed in equilibrium (kg m^{-3})
K	equilibrium constant of the adsorption isotherm
k	specific velocity of Hg fixation (m^3 kg^{-1} s)
Rp	particle radius (m)
D	diffusivity (m^2 s)
L	bed length (m)
z	axial coordinate (m)
r	radial coordinate (m)
υ	linear velocity of the gas (m s^{-1})
t	time (h)
T	temperature (K)
m	sorbent weight (kg)
S	value of optimized objective function
NE	number of experimental points
n	number of discretizationboxes
ρ_p	particle density (kg m^{-3})
ρ_b	bed density (kg m^{-3})
ε	porosity

Abbreviations

PSO	Particle Swarm Optimization
SQP	Sequential Quadratic Programming
HAp	hydroxyapatite

PSO parameters

N_{pt}	number of points
N_{iter}	number of iterations
w	initial inertial value
c_1	cognition parameter
c_2	social parameter
TOL	tolerance

Dimensionless numbers

σ	constant
Γ	dimensionless mercury concentration in the fluid phase
Γ_i^C	calculated dimensionless concentration in the fluid phase at the outlet of the bed
Γ_i^E	experimental dimensionless concentration in the fluid phase at the outlet of the bed
τ	dimensionless time
ϖ	relation between convective and diffusive terms
ξ	dimensionless length
ψ	dimensionless mercury concentration in the solid phase
ϕ	relation between reactive and diffusive terms
λ	dimensionless related to available sites for mercury fixation
κ	dimensionless isotherm constant
λ_{max}	dimensionless of maximum fixation capacity

elemental form [1]. Furthermore, mercury is a substance which has been focus of many studies due to its adverse effects on human health, high toxicity and bioaccumulative properties.

On natural gas, typical concentrations of mercury are between 1 and 200 μg m^{-3} [4]. However, there is a significant spatial–temporal variability of mercury concentration in natural gas [5,6] and high amounts of this fuel are processed annually around the world. Therefore, mercury emissions from natural gas require control even though the low mercury concentrations. Furthermore, mercury corrosion is associated with serious failures at natural gas plants [4].

Mercury emissions occur in three forms: elemental mercury (Hg^0), oxidized mercury (Hg^{2+}) and particle-bound mercury (Hg^p) [7]. Elemental mercury is the major chemical form emitted to the atmosphere [8] and it is difficult to capture by the existing air pollution control devices due to both water insolubility and high volatility [9].

Adsorption onto carbon, activated carbon, halide- and sulfur-impregnated activated carbon [10–13], transition metal oxides [14], and supported noble metals have been reported in the literature [15]. The stability of captured mercury is an important issue and desired characteristic of the sorbent, knowing the environmental risks associated with sorbent disposal at the end of adsorption process. Some recent studies have investigated sorbents with ability to retain mercury in stable form [16]. However, only a few studies have focused on modeling the adsorption-fixation mercury from gaseous stream. Chung et al. [17]applied the modeling assuming to different active sites for mercury adsorption on impregnated activated carbon. Ren et al. [18] developed a model based on the mechanism of surface equilibrium and mass transfer, and this model can be used to determine the effects of sorbent properties on mercury removal at different conditions. None of previous model includes, besides adsorption, the Hg fixation process explicitly.

Here, we provide a model based on the mercury sorption process involving the surface adsorption, the diffusion into the sorbent particle, and the chemical reaction into the solid matrix. The chemical reaction mechanism is added to the model aiming to explain the high mercury fixation capacity of our sorbents, which was previously confirmed by stabilization results to lixiviation and thermal treatment tests. Very low leaching of mercury in water (pH = 5) and no Hg release at high temperatures (up to 60 °C) were observed [19]. Simulations using the proposed model are performed to observe the influence of mercury-fixation on the dynamics behavior of the fixed-bed column.

2. Experimental section

2.1. Sorbents

Two different adsorbents developed in our laboratory are used here: sorbent A (Case 1) and B (Case 2). Both sorbents are synthetic non-stoichiometric hydroxyapatites (HAp), $Ca_{10-z}(HPO_4)_z(PO_4)_{6-z}(OH)_{2-z}$ [$0 < z < 1$], modified with different copper content (5.4% to solid A and 2.3% to solid B). Hydroxyapatite precursor of sorbent A was prepared by the precipitation method and copper incorporation was performed by the ion exchange method. These methods were described to zinc modified hydroxyapatites in previous work [20], but copper instead of zinc is used in the present work. Sorbent B was prepared by co-precipitation method: copper incorporation already occurs in hydroxyapatite preparation substituting part of calcium nitrate used in hydroxyapatite precipitation by copper nitrate. Both sorbents (A and B) were exposed to a stream with 5%

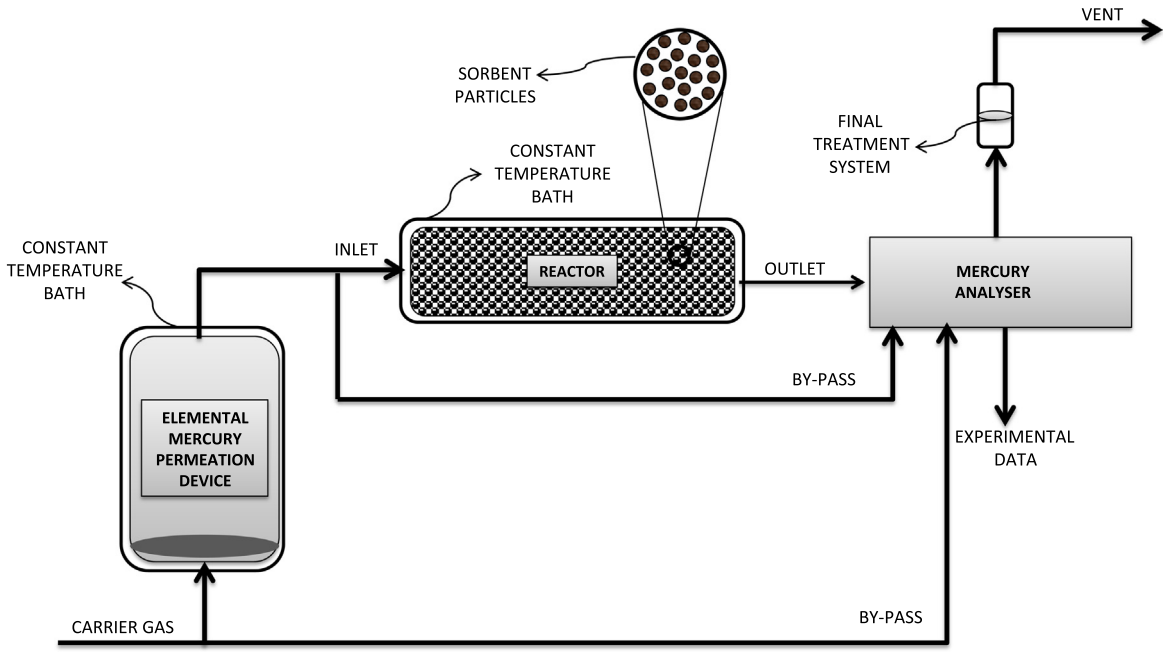

Fig. 1. Schematic diagram of the bench-scale fixed-bed reactor.

H_2S diluted in helium for 2 h in a sulfidation process, in order to activate the mercury removal sites.

2.2. Sorption experiments

The Hg^0 adsorption study was performed in a fixed-bed column shown in Fig. 1. The gaseous stream containing low mercury concentrations flows, at a given temperature, through the column filled up with hydroxyapatite sorbent. Keeping the saturator temperature constant during the experiment, the inlet mercury concentration is controlled.

The experimental conditions of the Case 1 and Case 2 are shown in Table 1. Methane was chosen to simulate the natural gas in Case 1 once it is the major component of this fuel and, consequently, natural gas properties are very similar to those of methane [21]. Nitrogen (N_2) is used as a carrier gas to focus only on mercury removal in Case 2.

2.3. Sorbent characterization

X-ray diffraction (XRD) analyses are performed in order to investigate crystalline structures of the fresh sorbent (before adsorption) and the used sorbent (after adsorption). The XRD analyses are carried out on X-ray diffractometer (Rigaku DMax 2200 Diffractometer) using Cu Kα radiation. The scanning ranged from 5° to 80° (2θ) with a size step of 0.02° and time step of 5s. Diffraction patterns are refined using the Rietveld method [22] and the hydroxyapatite model based on Wilson et al. [23] experimental data.

XRD experimental results obtained for fresh hydroxyapatite (sorbent precursor) (HAp), hydroxyapatite modified with copper (Cu-HAp), and used sorbent (after mercury adsorption) are shown in Fig. 2. Hydroxyapatite phase is identified in Hap (A) and Cu-Hap (B)samples, however cell parameters were changed when copper is added (A: $a = 9.42505 \pm 0.00036$ and $c = 6.87866 \pm 0.00027$, B:

Table 1
Summary of the experimental conditions.

Property	Parameter	Unit	Case 1	Case 2
Temperature of the reactor	T	K	301	301
Bed length	L	m	0.005	0.01
Linear velocity	υ	m s^{-1}	6.4×10^{-3}	6.4×10^{-3}
Inlet mercury concentration	C_o	kg m^{-3}	1.25×10^{-5}	9.34×10^{-6}
Particle density	ρ_p	kg m^{-3}	2.61×10^{3}	2.61×10^{3}
Bed density	ρ_b	kg m^{-3}	6.37×10^{2}	6.37×10^{2}
Bed porosity	ε	–	0.75	0.75
Sorbent weight	m	kg	2.5×10^{-4}	5×10^{-4}
Metal loading of sorbent	–	%	5.4	2.3
Maximum fixation capacity	q_{RQm}	kg m^{-3}	221	95

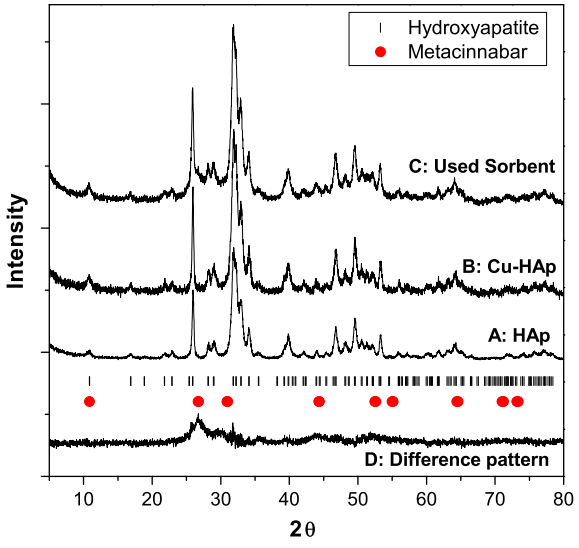

Fig. 2. XRD patterns for samples of hydroxyapatite (sorbent precursor) (A: HAp), hydroxyapatite modified with copper (B: Cu-Hap), and for used sorbent (C). The new phase containing mercury (metacinnabar, HgS) is shown in the diffraction pattern (D) obtained from the difference between the synthetic HAp and used sorbent.

$a = 9.41630 \pm 0.00054$ and $c = 6.87521 \pm 0.00040$). These changes on the unit cell parameters suggest that the copper is incorporated to the hydroxyapatite structure.

We have refined the diffraction pattern of modified hydroxyapatites by using a single-phase hydroxyapatite model [23] and the difference in patterns presented by those solids. Characteristic diffraction peaks of metacinnabar (HgS) phase are presented in Fig. 2. From these comparisons, we propose that the Hg^0 sorption mechanism includes the reaction between Cu_xS_y – HAp(s) and $Hg^0(g)$ to form HgS(s). The formation of this stable mercury compound explains the high mercury fixation observed here for our sorbents.

3. Mathematical modeling for Hg^0 removal

3.1. Combining sorption-reaction mechanisms

The proposed model to describe the mercury removal from gaseous streams using modified hydroxyapatites is based on the following assumptions:

(1) The process is isothermal and the adsorption isotherm is linear. These assumptions are acceptable because the adsorbate is presented in very low concentration [24,25].
(2) The fixation process can be described by a first-order chemical reaction.
(3) The chemical reaction is limited by a maximum fixation capacity defined for each specific solid.
(4) The concentration profile within a spherical sorbent particle is parabolic [24,26].
(5) Both axial dispersion and pressure drop through the column are negligible.

Based on these assumptions, the process is shown in a schematic diagram of Fig. 3.

3.2. Model equations

In accordance with previous hypotheses, the solute material balances in a bed volume element is

$$\frac{\partial C}{\partial t} + \upsilon \cdot \frac{\partial C}{\partial z} + \frac{(1-\varepsilon)}{\varepsilon} \cdot \frac{\partial \bar{q}}{\partial t} + \frac{(1-\varepsilon)}{\varepsilon} \cdot \frac{\partial q_{RQ}}{\partial t} = 0 \quad (1)$$

where C and $\bar{q}$ are solute concentration in the fluid phase and the average solute concentration inside the particles, respectively; υ is the linear velocity of the gas; ε is the bed porosity; z is the axial coordinate; t is time; q_{RQ} and q_{RQm} represent the amount of mercury already reacted per unit volume at time t and the corresponding maximum fixation capacity of the specific sorbent.

The boundary condition used to solute mass balance in fluid phase is the constant inlet Hg concentration (C_o):

$$C(z=0,t) = C_o \quad (2)$$

The average Hg concentration ($\bar{q}$) inside the spherical particle is given by:

$$\bar{q} = \frac{3}{Rp} \cdot \int_0^{Rp} (q \cdot r^2) dr \quad (3)$$

where q is the solute concentration inside the particles; Rp is the particle radius; and r is the radial coordinate inside the particle.

Differentiating Eq. (3) with respect to time, we obtain Eq. (4).

$$\frac{\partial \bar{q}}{\partial t} = \frac{3}{Rp} \cdot \int_0^{Rp} \left[\left(\frac{\partial q}{\partial t} \right) \cdot r^2 \right] dr \quad (4)$$

In our proposed model, the term $\left(\frac{\partial q}{\partial t}\right)$ involves the diffusion process and the first-order chemical reaction inside the particle, associated with the mercury fixation mechanism in the solid (Eq. (5)).

$$\frac{\partial q}{\partial t} = \frac{D}{Rp^2} \cdot \frac{\partial}{\partial r} \left(r^2 \cdot \frac{\partial q}{\partial r} \right) - k \cdot (q_{RQm} - q_{RQ}) \cdot q \quad (5)$$

where D is the diffusivity; k is the specific velocity of this chemical reaction; and q_{RQm} is the maximum amount of mercury that can be fixed by the sorbent.

From Eqs. (4) and (5), we have (assuming constant diffusivity):

$$\frac{\partial \bar{q}}{\partial t} = \frac{3 \cdot D}{Rp} \cdot \left(\frac{\partial q}{\partial r} \right)_{r=Rp} \quad (6)$$

By assuming the parabolic Hg concentration profile inside the sorbent particle (Eq. (7)) and by satisfying the symmetry condition (Eq. (8)), we obtain the Eq. (9), at the point $r = Rp$:

$$q = a_o + a_2 \cdot r^2 \quad (7)$$

$$\left. \frac{\partial q}{\partial r} \right|_{r=o} = 0 \quad (8)$$

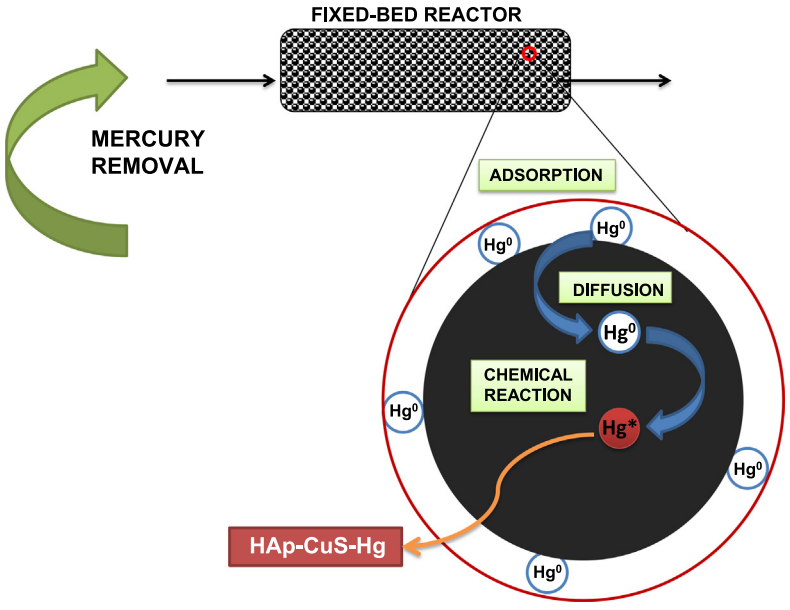

Fig. 3. Proposed model for mercury sorption into modified with copper sulfide hydroxyapatites.

$$\left(\frac{\partial q}{\partial r}\right)_{r=Rp} = \frac{5}{Rp}\cdot(q_{Rp}-\bar{q}) \tag{9}$$

From Eqs. (6) and (9), we have:

$$\frac{\partial \bar{q}}{\partial t} = \frac{15\cdot D}{Rp^2}\cdot(q_{Rp}-\bar{q}) - k\cdot(q_{RQm}-q_{RQ})\cdot\bar{q} \tag{10}$$

In Eqs. (9) and (10), q_{Rp} is the Hg concentration adsorbed at the interface in equilibrium with the gas-phase concentration (C). In this work, the linear isotherm is used, as shown:

$$q_{Rp} = K\cdot C \tag{11}$$

where K is the equilibrium constant (Henry constant) of the adsorption isotherm.

The chemical reaction rate (fixation) is

$$\frac{\partial q_{RQ}}{\partial t} = k\cdot(q_{RQm}-q_{RQ})\bar{q} \tag{12}$$

In this modeling, q_{RQm} is estimated from the copper content for each sorbent considering a stoichiometric Cu/S ratio equal to 2:1. We also assume both complete cooper sulfidation and total availability of sites for mercury fixation. We have obtained values of q_{RQm} = 221 kg m^{-3} for Case 1 and q_{RQm} = 95 kg m^{-3} for Case 2."

The initial conditions for breakthrough curve calculation are

$$C(z,t=0) = 0 \qquad 0 \leqslant z \leqslant L \tag{13}$$

$$\bar{q}(z,t=0) = 0 \qquad 0 \leqslant z \leqslant L \tag{14}$$

$$q_{RQ}(z,t=0) = 0 \qquad 0 \leqslant z \leqslant L \tag{15}$$

3.3. Normalization

In order to reduce both the number of parameters and the computational effort, we define the following dimensionless variables. In these equations, Γ, ψ, λ, ξ, and τ are the dimensionless variables related with the gas-phase concentration, the solid-phase concentration, the number of available sites for mercury fixation, the bed length and the time, respectively; L is the bed length, ξ is the dimensionless length, λ_{max} is the dimensionless of maximum fixation capacity and σ is an arbitrary constant. The dimensionless parameters ϖ, ϕ and κ represent the relation between convective and diffusive terms, the relation between reactive and diffusive term and the isotherm constant, respectively.

$$\tau = 15\cdot D\cdot t/Rp^2 \tag{16}$$

$$\xi = z/L \tag{17}$$

$$\Gamma = C/C_o \tag{18}$$

$$\psi = \bar{q}\cdot(1-\varepsilon)/(\sigma\cdot\varepsilon\cdot C_o) \tag{19}$$

$$\lambda = (q_{RQm}-q_{RQ})/q_{RQm} \tag{20}$$

$$\lambda_{max} = q_{RQm}\cdot(1-\varepsilon)/(\sigma\cdot\varepsilon\cdot C_o) \tag{21}$$

$$\varpi = \upsilon\cdot Rp^2/(\sigma\cdot 15\cdot D\cdot L) \tag{22}$$

$$\phi = k\cdot Rp^2\cdot q_{RQm}/(15\cdot D) \tag{23}$$

$$\kappa = K\cdot(1-\varepsilon)/(\sigma\cdot\varepsilon) \tag{24}$$

Thus the complete dimensionless model, consisting of material balance, the solid-phase material balance, and the rate of fixation reaction is as follows

$$\frac{1}{\sigma}\cdot\frac{\partial\Gamma}{\partial\tau} + \varpi\cdot\frac{\partial\Gamma}{\partial\xi} + \kappa\cdot\Gamma - \psi = 0 \tag{25}$$

$$\frac{\partial\psi}{\partial\tau} = \kappa\cdot\Gamma - \psi - \phi\cdot\psi\cdot\lambda \tag{26}$$

$$\frac{\partial\lambda}{\partial\tau} = -\frac{\phi\cdot\psi\cdot\lambda}{\lambda_{max}} \tag{27}$$

The boundary and the initial conditions for breakthrough curve calculation, in the dimensionless form, are

$$\Gamma(\xi=0,\tau) = 1 \tag{28}$$

$$\Gamma(\xi,\tau=0) = 0 \qquad 0 \leqslant \xi \leqslant 1 \tag{29}$$

$$\psi(\xi,\tau=0) = 0 \qquad 0 \leqslant \xi \leqslant 1 \tag{30}$$

$$\lambda(\xi,\tau=0) = 1 \qquad 0 \leqslant \xi \leqslant 1 \tag{31}$$

3.4. Parameters estimation procedure

In order to reduce the partial differential equations into ordinary differential equations, the bed length is discretized by finite differences method, dividing the column length in n = 100 equal boxes. The arbitrary variable $\sigma = 10^6$ is chosen to maintain the magnitude of the non-dimensional variables near unit.

The model is integrated in the software Matlab through an implementation of an implicit Runge–Kutta formula using trapezoidal rule step and a backward, second-order differentiation formula, consecutively [27].

The model parameters are obtained from fitting procedure of experimental data through coupled optimization runs of an objective function. The use of deterministic method in the optimization procedure provides a faster convergence of the parameter values, however it requires a good approximation for initial parameters. Heuristic methods have the advantage of being able to find the global minimum, independent of the initial parameters. In addition, according to Schwaab et al. [28], these methods require less computational effort because they do not need derivatives of the objective function. Here, we have used a hybrid method combining the Particle Swarm Optimization (PSO), heuristic algorithm, and a Newton-like method. The parameter values obtained with the PSO are used as initial parameters for the minimization carried out through the deterministic, Newton-like, method.

The PSO method is based on gregarious behavior of animals assuming individuals (particles) moves within the search region, which is defined by the users. The evaluation of the objective function is made to each particle and the lowest result is stored. Exchanging information between particles is done in accordance with equations which involving the (pseudo) velocity and position of these particles, the search direction and the number of iteration. Random values with uniform distribution in the range [0–1] and search parameters *Npt* (number of points), *Niter* (number of iterations), *c1* and *c2* (cognition and social parameters), *TOL* (tolerance)

Table 2
Input parameters of the PSO algorithm.

Parameter	Value
Npt	50
Niter	10^3
c1	1
c2	1
w	0.75
TOL	10^{-3}

and initial value of w (initial inertial weight) are also used according to Table 2. Details of this method are described elsewhere [29].

Several values of objective function, evaluated during the optimization process, can be used to construct the confidence region in order to verify the correlation between the obtained parameters [28].

The software Matlab® is used in the implementation of heuristic and deterministic coupled methods. The Matlab® function "fmincon" is employed as a deterministic method in the optimization of constrained nonlinear multivariable function. Here it is chosen the SQP (Sequential Quadratic Programming) algorithm that uses a quasi-Newton approximation to the Hessian.

Assuming that the model is perfect, the experiments are well done, the experimental errors have normal distribution, the experimental measurements of the dependents variables are uncorrelated, and the variances of the experimental fluctuations of the dependent variables are equal, the unweighted least-squares function [26] could be employed as an objective function:

$$S = \sum_{i=1}^{NE} \left(\Gamma_i^C - \Gamma_i^E\right)^2 \tag{32}$$

where NE is the number of experiments. The dimensionless concentrations at the outlet of the bed, Γ_i^C, are calculated at same times of the dimensionless experimental data points, Γ_i^E.

4. Breakthrough curves results

Experimental breakthrough data are obtained under different operational conditions for two different sorbents (Case 1 and Case 2). These experimental data are used to obtain the parameters of the proposed model. For each case, we have obtained three parameters in non-dimensional form, related to the diffusivity and the particle radius, the equilibrium constant of the adsorption isotherm, and the specific velocity of the mercury fixation into de solid matrix, respectively. The optimized objective function (S) and the three parameters (ϖ, κ and ϕ) are shown in Table 3 for both cases studied here.

Experimental and calculated breakthrough curves for Cases 1 and 2 are plotted in Fig. 4(a). For both cases, calculated breakthrough curves are in good agreement with experimental data. In common we notice that no complete saturations are achieved, at least on the time scale observed, due to the Hg fixation process (chemical reaction mechanism). From this figure, we can also observe that the affinity of Hg-sorbent is higher for Case 2, comparing with Case 1.

Because the bed length is higher for Case 2 than Case 1, dimensionless group $\left(\frac{t.v}{L}\right)$ is used in abscissa axis, (Fig. 4(b), in order to eliminate the bed-length effect. Although higher Hg retention is observed for Case 1 at short timescale, more related with different diffusivities (higher ϖ value for Case 2), the breakthrough curves still show large Hg-sorbent affinity at large timescale.

The confidence regions for all estimated parameters for Case 1 are shown in Fig. 5. Because of the elliptic shape shown for each pair of parameters, we can affirm that those parameters are not strongly correlated. Similar results, not shown here, are observed for Case 2.

Table 3
Optimized objective function and parameters obtained by the hybrid optimization method.

	S	ϖ	κ	ϕ
Case 1	0.0479	0.0424	1.9474	0.0016
Case 2	0.0224	0.2495	2.5089	0.0314

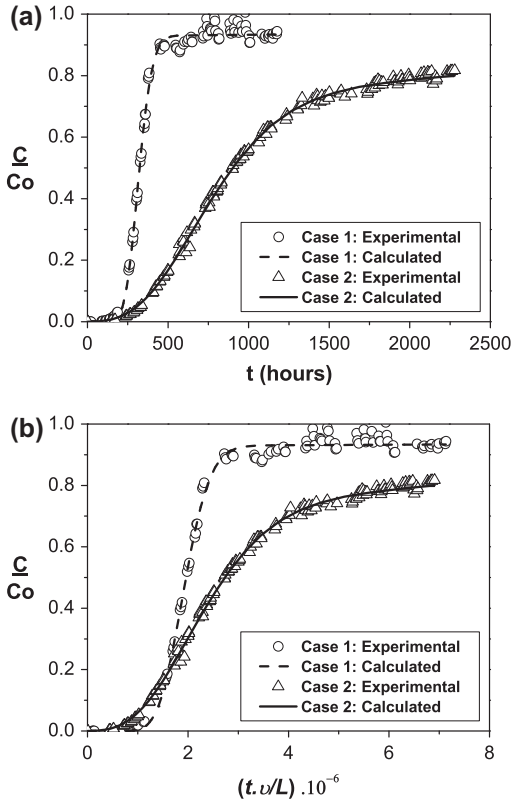

Fig. 4. Comparison of experimental and calculated breakthrough curves for Cases 1 and 2 using (a) time (hours) and (b) $\left(\frac{t.v}{L}\right)$ dimensionless group.

5. Investigation of the adsorption dynamics behavior

5.1. Analysis of chemical reaction

The proposed model is used to observe the influence of the fixation chemical reaction parameter (ϕ) on breakthrough curves. High value of ϕ means an increase chemical reaction rate comparing to diffusive process.

As shown in Fig. 6, adsorption process has dominant effect at early stages of adsorption, in such a way that there is no difference between curves even for very different ϕ values. However, chemical reaction effect is important for larger timescale and the capacity of mercury removal increases for higher chemical reaction ϕ value.

5.2. Adsorption column dynamics behavior during operational discontinuation

The proposed model is used to study the dynamics of adsorption column caused by two operational conditions: discontinuation in mercury feed concentration and flow interruption of gas stream. The occurrence of interruptions and/or discontinuation in the gas stream and mercury concentration is simulated to evaluate the possibility of using this solid in real processes. In order to prevent numerical problems and to better describe a real operational interruption during process operation, a first-order exponential function, as a regularization function instead of applying a step function, is used.

Fig. 7 shows the influence of gas stream feed interruption on the breakthrough curves. Interruptions are programmed to occur at 25th day of operation for the Case 1 and at 50th day for the Case 2 and those interruptions are maintained for periods of time of 100 days and 200 days, respectively.

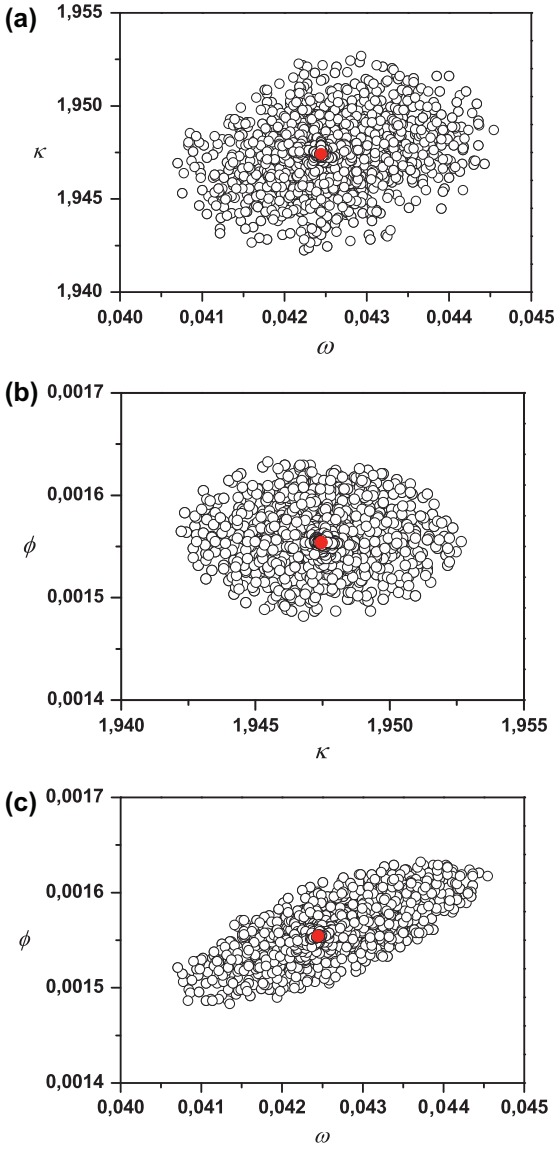

Fig. 5. Confidence region determined using particle swarm optimization method for each pair of the parameters obtained for Case 1.

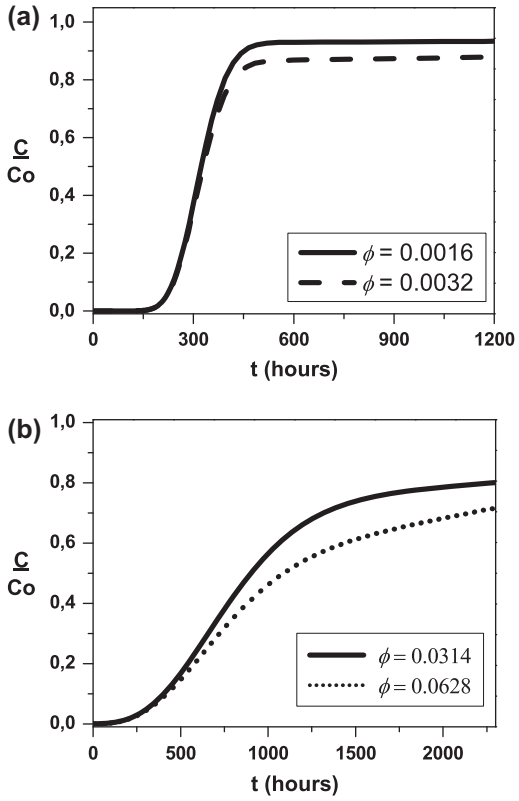

Fig. 6. Comparison between the breakthrough curves obtained with the optimized value of ϕ and with twice its value for (a) Case 1 and (b) Case 2.

The interruption provides the sufficient time to both diffusion and mercury fixation occurrence and an important decrease in the outlet mercury concentration is observed when the feed is turned back, when compared with concentration when occurs the feed interruption. This behavior is associated with the fixation of mercury into the sorbent and consequent renovation of adsorption surface. Therefore, chemical fixation leads to a significant increase of mercury removal, provided that the timescale is appropriate.

Fig. 8 shows the influence of interruptions of the mercury feed concentration on the breakthrough curves. Mercury feed concentration is turned on and turned off in a cycle of 20 days for Case 1 and 100 days for Case 2. This sequence is repeated for three series of similar runs. During the interruption time the mercury concentration in the inlet of the bed is zero. However, even during this time the dimensionless parameters Γ and λ_{max} are calculated using the non-zero value of C_o as indicated in Table 1.

We observe an oscillation in the mercury outlet concentration due to the periodic interruption of the inlet Hg concentration. A decrease on fluid concentration due to mercury fixation into the adsorbent particle is observed, however, this reaction does not

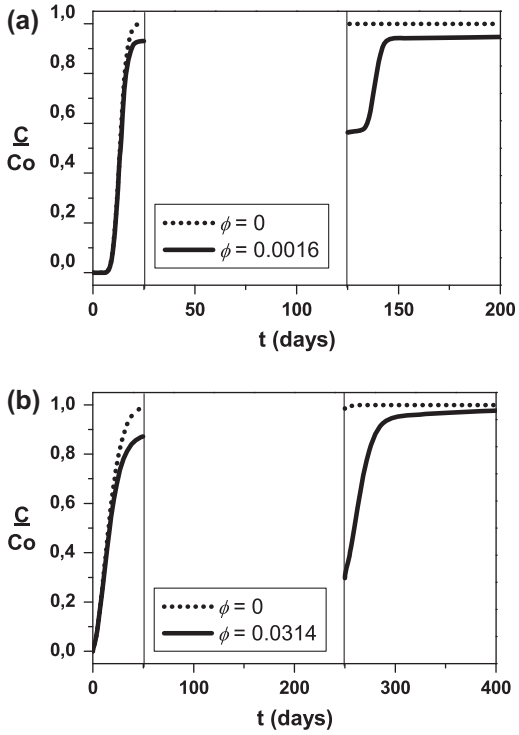

Fig. 7. Comparison between breakthrough curves obtained for simulated interruptions on the gaseous stream. For the Case 1 (a), interruptions of 100 days after 25 days of operation in absence ($\phi = 0$) and presence ($\phi = 0.0016$) of chemical reaction. For Case 2 (b), interruptions of 200 days after 50 days of operation in absence ($\phi = 0$) and presence ($\phi = 0.0314$) of chemical reaction.

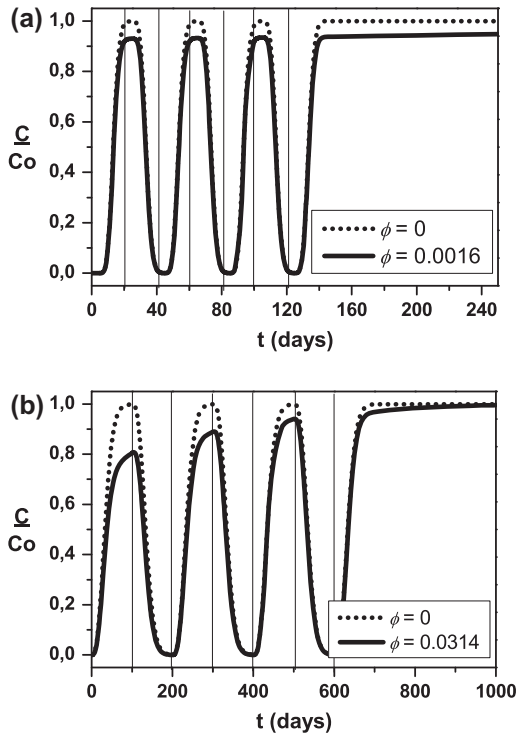

Fig. 8. Comparison of the breakthrough curves obtained for simulated interruptions on the mercury feed. For the Case 1 (a), three cycles with 20 days of each interruption in absence ($\phi = 0$) and presence ($\phi = 0.0016$) of chemical reaction $C_0 = 1.25 \times 10^{-5}$ kg m^{-3}. For the Case 2, three cycles with 100 days of each interruption in absence ($\phi = 0$) and presence ($\phi = 0.0314$) of chemical reaction ($C_0 = 9.34 \times 10^{-6}$ kg m^{-3}).

change the wave period. In this case, due to the timescale of each cycle, the advective process is responsible for the concentration behavior. Notice that the gaseous stream remains passing through the bed during whole time. In addition, the mercury already incorporated into the particle can return to the fluid phase maintaining the equilibrium of the mercury concentration between solid and fluid. When the chemical reaction is present, this effect is minimized because the mercury stays fixed into the solid matrix.

Although the maximum fixation capacity (q_{RQm}) in Case 2 is lower than that in Case 1, the effect of chemical reaction occurrence is more evident due to the higher value of ϕ (0.0016 and 0.0314 to Case 1 and 2, respectively). In Case 2, the reduction of this effect at each cycle occurs as the chemical fixation sites are filled. For Case 1, this reduction is not noted in the studied timescale owing to higher metal loading of Sorbent A (Fig. 2) and, consequently, higher q_{RQm} value.

6. Conclusions

We provide a study of mercury removal from gaseous streams by adsorption process using two different synthetic hydroxyapatites developed in our laboratory, which have high ability to fix mercury into the solid matrix. A mathematical model is presented that taking into account mercury adsorption, its diffusion and fixation chemical reaction into the sorbent particles. The hypothesized mechanism has been confirmed by DRX analyses, indicating mercury sulfide phase formation. Dimensionless parameters of the model related to these phenomena are obtained by minimization of the least-squares function using a hybrid optimization method. Parameters are $\varpi = 0.0424$, $\kappa = 1.9474$, $\phi = 0.0016$ for Case 1 and $\varpi = 0.2495$, $\kappa = 2.5089$, $\phi = 0.0314$ for Case 2. We have shown that these parameters are uncorrelated for both cases.

An investigation of the importance of the chemical reaction on the breakthrough curves shows that the mercury removal capacity is proportional to kinetic constant of the mercury-solid reaction. Dynamics behavior of the adsorption column suggests that the interruptions on gaseous stream feed leads to an important increasing of mercury removal capacity, providing an appropriate timescale.

This study suggests that a scale-up of this process could be useful. The amount of final residue of the process would be minimized and the mercury would remain fixed on used sorbent even after its disposal.

Acknowledgements

The authors would like to dedicate this paper to Professor Alberto Luiz Coimbra, in the 50th anniversary of COPPE (1963–2013), the Graduate School of Engineering of the Federal University of Rio de Janeiro.

References

[1] UNEP Chemicals Branch. The global atmospheric mercury assessment: sources, emissions and transport. UNEP-Chemicals, Geneva, Switzerland; 2008.
[2] Liu J, Qu W, Joo SW, Zheng C. Effect of SO_2 on mercury binding on carbonaceous surfaces. Chem Eng J 2012;184:163–7.
[3] Nelson PF, Morrison AL, Malfroy HJ, Cope M, Lee S, Hibberd ML, et al. Atmospheric mercury emissions in Australia from anthropogenic, natural and recycled sources. Atmos Environ 2012;62:291–302.
[4] Shafawi A, Ebdon L, Foulkes M, Stockwell P, Corns W. Determination of total mercury in hydrocarbons and natural gas condensate by atomic fluorescence spectrometry. Analyst 1999;124:185–9.
[5] Ryzhov VV, Mashyanov NR, Ozerova NA, Pogarev SE. Regular variations of the mercury concentration in natural gas. Sci Total Environ 2003;304:145–52.
[6] Vaisman AG, Lacerda LD. Estimated heavy metal emissions to the atmosphere due to projected changes in the Brazilian energy generation matrix. Reg Environ Chan 2003;3:140–5.
[7] Zhuang Y, Zygarlicke CJ, Galbreath KC, Thompson JS, Holmes MJ, Pavlish JH. Kinetic transformation of mercury in coal combustion flue gas in a bench-scale entrained-flow reactor. Fuel Process Technol 2004;85:463–72.
[8] Pacyna EG, Pacyna JM. Global emission of mercury from anthropogenic sources in 1995. Water Ar Soil Poll 2002;137:149–65.
[9] Liu L, Duan Y, Wang Y, Wang H, Yin J. Experimental study on mercury release behavior and speciation during pyrolysis of two different coals. J Fuel Chem Technol 2010;38:134–9.
[10] Yang H, Xu Z, Fan M, Bland AE, Judkins RR. Adsorbents for capturing mercury in coal-fired boiler flue gas. J Hazard Mater 2007;146:1–11.
[11] His H-C, Chen C-T. Influences of acidic/oxidizing gases on elemental mercury adsorption equilibrium and kinetics of sulfur-impregnated activated carbon. Fuel 2012;98:229–35.
[12] Sasmaz E, Kirchofer A, Jew AD, Saha A, Abram D, Jaramillo TF, et al. Mercury chemistry on brominated activated carbon. Fuel 2012;99:188–96.
[13] Wade CB, Thurman C, Freas W, Student J, Matty D, Mohanty DK. Preparation and characterization of high efficiency modified activated carbon for the capture of mercury from flue gas in coal-fired power plants. Fuel Process Technol 2012;97:107–17.
[14] Guo P, Guo X, Zheng C. Roles of γ-Fe_2O_3 in fly ash for mercury removal: results of density functional theory study. Appl Surf Sci 2010;256:6991–6.
[15] Baltrus JP, Granite EJ, Pennline HW, Stanko D, Hamilton H, Rowsell L, et al. Surface characterization of palladium–alumina sorbents for high-temperature capture of mercury and arsenic from fuel gas. Fuel 2010;89:1323–5.
[16] Graydon JW, Zhang X, Kirk DW, Jia CQ. Sorption and stability of mercury on activated carbon for emission control. J Hazard Mater 2009;168:978–82.
[17] Chung ST, Kim KI, Yun YR. Adsorption of elemental mercury vapor by impregnated activated carbon from a commercial respirator cartridge. Powder Technol 2009;192:47–53.
[18] Ren J, Zhou J, Luo Z, Zhong Y. Fixed-bed experiments and mathematical modeling for adsorption of mercury vapor. Chall Power Eng Environ 2007;1:843–9.
[19] Resende NS, Salim VMM. Hg species immobilization by metal doped calcium phosphate. In. 10th International conference on mercury as a global pollutant, Nova Scotia, Canada; 2011.
[20] Faria RMB, César DV, Salim VMM. Surface reactivity of zinc-modified hydroxyapatite. Catal Today 2008;133–5:168–73.
[21] Karavalakis G, Durbin TD, Villela M, Miller JW. Air Pollutant emissions of light-duty vehicles operating on various natural gas compositions. J Nat Gas Sci Eng 2012;4:8–16.
[22] Rietveld HM. A profile refinement method for nuclear and magnetic structures. J Appl Cryst 1969;2:65–71.
[23] Wilson RM, Elliot JC, Dowker SEP. Rietveld refinement of the crystallographic structure of human dental enamel apatites. Am Miner 1999;84:1406–14.

[24] Ruthven DM, Farooq S, Knaebel KS. Pressure swing adsorption. New York: VCH Publishers; 1994.
[25] Ruthven DM. Principles of adsorption & adsorption processes. New York: John Wiley & Sons; 1984.
[26] Yang RT. Gas separation by adsorption processes. Boston: Butterworths; 1987.
[27] Hosea ME, Shampine LF. Analysis and implementation of TR-BDF2. Appl Numer Math 1996;20:21–37.
[28] Schwaab M, Biscaia Jr EC, Monteiro JL, Pinto JC. Nonlinear parameter estimation through particle swarm optimization. Chem Eng Sci 2008;63:1542–52.
[29] Prata DM, Schwaab M, Lima EL, Pinto JC. Nonlinear dynamic data reconciliation and parameter estimation through particle swarm optimization: application for an industrial polypropylene reactor. Chem Eng Sci 2009;64:3953–67.